AFRL-SR-BL-TR-98-

0130

REPORT DOCUMENTATION PAGE

1. AGENCY USE ONLY (Leave blank)	2. REPORT DATE	3. REPORT TYPE AND DATES COVERED
		Final 01 Jul 96 to 31 Oct 97

4. TITLE AND SUBTITLE
Ultralow threshold Microlasers

5. FUNDING NUMBERS
61102F
2305/

6. AUTHOR(S)
Professor Levi

7. PERFORMING ORGANIZATION NAME(S) AND ADDRESS(ES)
University of Southern California
837 West 36th Place Sto-330
Los Angeles, CA 90089-1147

19980205 063

9. SPONSORING/MONITORING AGENCY NAME(S) AND ADDRESS(ES)
AFOSR/NE
110 Duncan Ave RoomB115
Bolling AFB DC 20332-8050

10. SPONSORING/MONITORING AGENCY REPORT NUMBER
F49620-96-1-0357

11. SUPPLEMENTARY NOTES

12a. DISTRIBUTION/AVAILABILITY STATEMENT
APPROVAL FOR PUBLIC RELEASED: DISTRIBUTION UNLIMITED

12b. DISTRIBUTION CODE

13. ABSTRACT (Maximum 200 words)

This final technical report summarizes advances to push the limits of ultralow thresold microlaser VCSEL design implementation, and performance. The main results are summarized:
1. Values of spontaneous emission coupling factor B in the range between 10-2 and 10-1 lead to comparatively low turn-on delay for both on-on and on-off modulation. Spontaneous emission factors lying between 10-2 and 10-1 are more attractive than devices with B-1.
2. With reduction of aperture size to less than 5x5 um2, the internal quantum efficiency decreases owing to carrier losses resulting from current spreading and carrier out-diffusion, the round-trip loss increases due to excess diffraction and scattering losses.
3. Modal noise and speckle visibility in Gb/s multimode waveguide interconnect systems depends on a complex interplay of carrier dynamics, spontaneous emission factor, gain compression, and device dimensions. Scaled low-power microlasers exhibit modal noise comparable to large incoherent multimode devices.
4. The series resistance of microlasers has been explored by fabricating low resistance, low-threshold current, intracavity-contacted devices.

17. SECURITY CLASSIFICATION OF REPORT	18. SECURITY CLASSIFICATION OF THIS PAGE	19. SECURITY CLASSIFICATION OF ABSTRACT	20. LIMITATION OF ABSTRACT
UNCLASSIFIED	UNCLASSIFIED	UNCLASSIFIED	UL

Final Technical Report

January 31, 1998.

Ultralow Threshold Microlasers

Award number #F49620-96-1-0357

Total project period July 1, 1996 to October 31, 1997

Agency contact: Dr. Alan Craig
AFOSR/NE
110 Duncan Av.
Bolling AFB, CD 20332-0001
voice 202-767-4934
fax 202-767-4986
email alan.craig@afosr.af.mil

Investigators:

Dr. A. F. J. Levi
University of Southern California
University Park, DRB 118
Los Angeles, CA 90089-1111
voice 213-740-7318
fax 213-740-9280
email alevi@usc.edu

Dr. P. D. Dapkus
University of Southern California
University Park, PHE 502
Los Angeles, CA 90089-0271
voice 213-740-4414
fax 213-740-6022
email dapkus@usc.edu

Summary:

This final technical report summarizes advances made at USC during the course of the 16 month program. Our main thrust is to push the limits of ultralow thresold microlaser design, implementation, and performance. The main results are summarized under the following four headings:

I. *Effect of scaling microlasers on jitter and turn-on delay* in which it is shown that values of spontaneous emission coupling factor β in the range between 10^{-2} and 10^{-1} lead to comparatively low turn-on jitter and turn-on delay for both on-on *and* on-off modulation. This demonstrates that microlasers with spontaneous emission factors lying between 10^{-2} and 10^{-1} are more attractive for practical applications requiring on-on *and* on-off modulation than devices with $\beta \sim 1$.

II. *Losses in Vertical Cavity Surface Emitting Lasers* have been explored experimentally and it is demonstrated that with reduction of aperture size to less than 5x5 μm^2, the internal quantum efficiency decreases owing to carrier losses resulting from current spreading and carrier out-diffusion, the round-trip loss increases due to excess diffraction and scattering losses. Carrier loss in native-oxide apertured VCSEL's is a significant limit to the scaling down of device performance

with aperture size for most reported VCSEL's confined by native-oxide so far, which have no intentional lateral confinement for carriers in the layers below current aperture.

III. *The effect of scaling microlasers on modal noise* has been successfully modeled and it is shown that modal noise and speckle visibility in Gb/s multimode waveguide interconnect systems depends on a complex interplay of carrier dynamics, spontaneous emission factor, gain compression, and device dimensions. Remarkably, these competing factors allow scaled low-power microlasers with optimized design and operating conditions to exhibit modal noise comparable to large incoherent multimode devices.

IV. *The series resistance of microlasers* has been explored experimentally. Models of behavior have been developed and verified by fabricating low resistance, low-threshold current, intracavity-contacted devices.

I. Effect of scaling microlasers on jitter and turn-on delay:

Recently there has been a great interest in fabricating scaled microlasers with low threshold current, high efficiency, and a large coupling of the spontaneous emission power into the lasing mode, leading to spontaneous emission factor, $\beta \sim 1$. Although the physics governing the behavior of such devices is of some interest, an important objective is to explore the effect of large β on turn-on delay and timing jitter for Non-Return to Zero (NRZ) signaling. This is of practical importance because turn-on delay and jitter ultimately affect system considerations such as bandwidth and bit error ratio (BER). We are able to show using numerical simulations that an optimal value of the spontaneous emission factor β lying between 0.01 and 0.1 exists. In this regime the turn-on delay and turn-on jitter for on-on *and* on-off modulation is minimized.

In our theoretical study we use the classical laser diode rate equations with Langevin noise source terms to phenomenological model a microlaser and estimate its turn-on delay and turn-on jitter. In our simulations, we modulate the current to the laser diode with a deterministic 1010.... signal at 1 Gb/s between a low current, I_{low}, and a high current, I_{high}. The mean turn-on delay, t_d, is the time needed to reach a total number of cavity photons S which is 50% of the difference in high and low steady-state values. Due to the random nature of spontaneous emission events, there is a distribution in the turn-on delay time. Turn-on jitter, σ, is calculated as the standard deviation of the distribution of t_d.

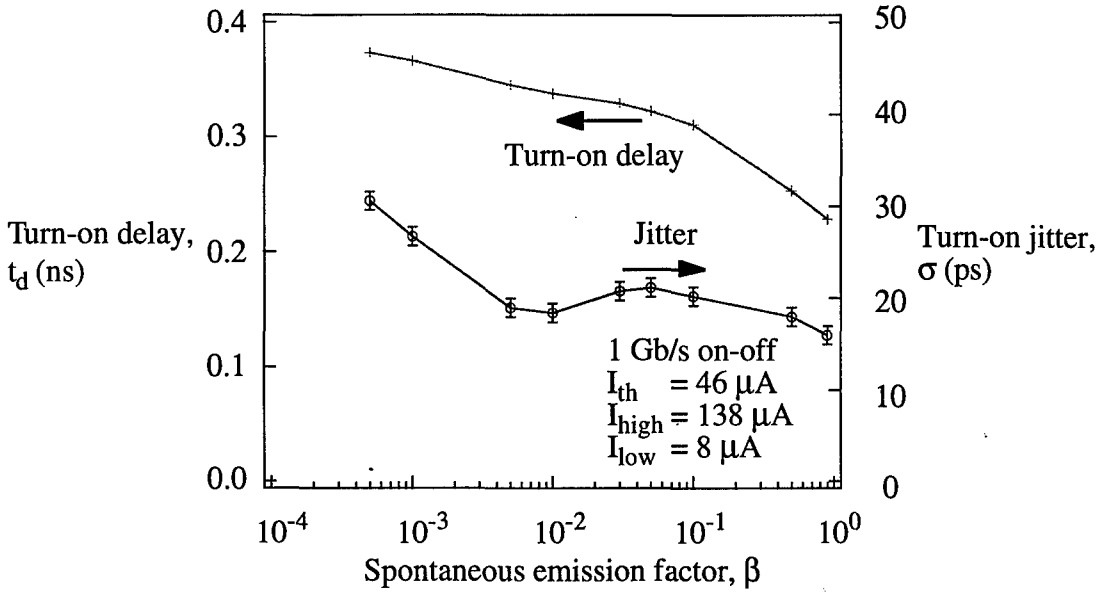

Figure 1 - Effect of spontaneous emission factor β on the turn-on delay and timing jitter for 1010... 1 Gb/s on-off modulation for a laser diode with I_{high} = 138 μA and I_{low} = 8 μA. The volume of the laser active region is $2X10^{-13}$ cm^3 and the threshold current is I_{th} = 46 μA.

Shown in Figure 1 is the dependence of the turn-on delay and jitter for an on-off modulated laser as a function of its spontaneous emission factor, β. The laser current is modulated between I_{low} = 8 μA and I_{high} = 138 μA. The threshold current for this device is I_{th} = 46 μA. The turn-on delay decreases monotonically with an increase in spontaneous emission factor. An increase in the spontaneous emission factor decreases the phase delay between the carriers and the photons. In the extreme limit of an LED, the photons follow the carrier density and hence the turn-on delay is minimized for a spontaneous emission factor of unity. Figure 1 also shows that the timing jitter does not monotonically increase or decrease with β. Jitter is due to the amount of noise and so depends directly on the amount of spontaneous emission coupling into the lasing mode. An increase in β increases the spontaneous emission noise and hence increases jitter. However, the total amount of noise also depends on the turn-on delay because that is the time for which noise is present. Hence, an increase in β also decreases the turn-on delay and hence decreases jitter. This is confirmed by the fact that the jitter does increase for $10^{-2} < \beta < 10^{-1}$ and the turn-on delay does not change significantly.

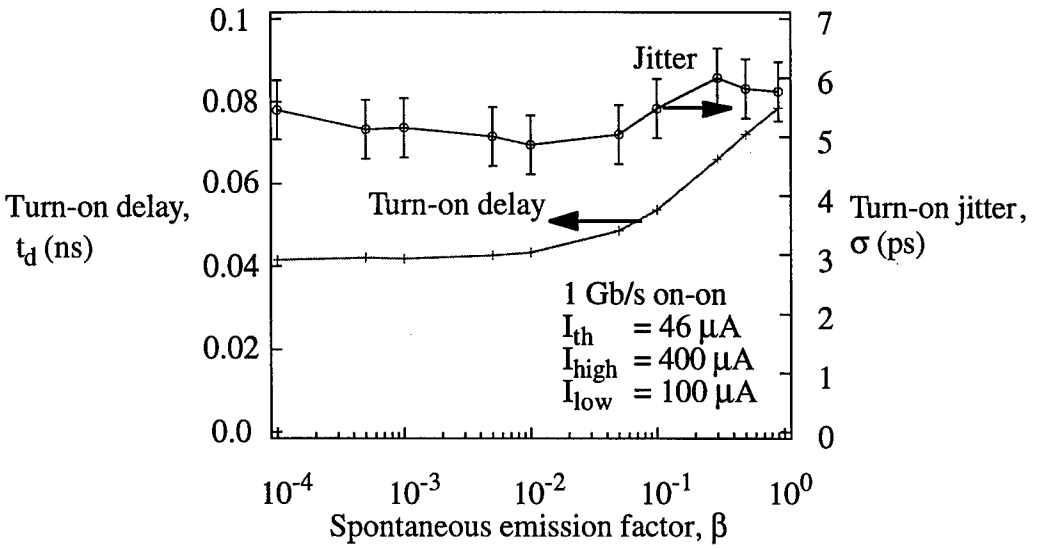

Figure 2 - Turn-on delay and jitter versus spontaneous emission factor β for on-on modulation for the device simulated in Figure 1. The laser current is toggled at 1 Gb/s between I_{high} = 400 μA and I_{low} = 100 μA.

Figure 2 shows the effect of β when the device is on-on modulated between I_{low} = 100 μA and I_{high} = 400 μA. The turn-on delay increases with an increase in β. This can be understood as follows: In the hypothetical case of a laser with β ~ 0 and on-on modulation, the turn-on time is limited by the stimulated emission time (~ ps). On the other hand, for a laser with β ~1, the turn-on time is affected by the carrier lifetime (~ 0.4 ns). Hence, the turn-on delay increases as the spontaneous emission factor, β, increases. Jitter is found to be approximately 5-6 ps for all the values of β. The small changes seen in the calculated values of jitter are attributed to the errors due to the pseudo-random number generator used and the finite number of samples (~ 800) used in calculating jitter.

From Figure 1 and Figure 2 one can readily see that a large β has a large turn-on delay for on-on modulation, although it gives a low jitter and turn-on delay for on-off modulation. On the other hand, a small value of β leads to a large turn-on delay for on-off modulation. Further, one can see that values of β in the range between 10^{-2} and 10^{-1} lead to comparatively low turn-on jitter and turn-on delay for both on-on *and* on-off modulation. This demonstrates that microlasers with spontaneous emission factors lying between 10^{-2} and 10^{-1} are more attractive for practical applications requiring on-on and on-off modulation than devices with β ~1.

II Losses in Vertical Cavity Surface Emitting Lasers

Vertical-cavity surface-emitting lasers (VCSEL's) with native oxide current apertures have resulted in threshold currents of semiconductor lasers in the range of tens of μA [1-4]. The ultralow thresholds result from a reduction of the active region volume and optical mode size through the current and optical field aperturing caused by the insulating and dielectric properties of the native-oxide, respectively. In a VCSEL with the native-oxide current constriction, the oxide layer and the aperture are intracavity elements so that some optical scattering and diffraction loss is expected at small apertures. Hegblom *et al.* [5] have estimated that the optical scattering loss becomes significant (~0.001 per pass) for small aperture sizes (~2 μm), where single-mode devices are still possible.

In addition to optical loss, carrier loss in native-oxide apertured VCSEL's may also be a significant factor that limits the extent to which the performance can be scaled with aperture size. In most VCSEL's confined by native-oxide, there is no intentional lateral confinement for carriers in the layers below current aperture. Lateral current spreading, low bias leakage currents in the regions outside the aperture and carrier out-diffusion are expected to become more important for smaller aperture sizes. Experimental results for AlAs native-oxide confined narrow-stripe edge-emitting lasers[6] suggests that these current and carrier losses limits the threshold current at small stripe width. In this paper, we present the characterization of current aperture size effect on internal quantum efficiency and round trip loss for AlAs native-oxide confined VCSEL's. AlAs native-oxide apertured VCSEL's, utilizing binary GaAs/AlAs DBR's, $In_{0.2}Ga_{0.8}As$ / GaAs resonant λ-cavity, and intracavity p-contact, have been fabricated with various aperture sizes. The dependence of internal quantum efficiency and round trip loss on current aperture size are assessed by removing layers of the top DBR's through selective etching to vary reflectivity.

The VCSEL's structure [3] in our study consists of a 30-pair n-doped AlAs/GaAs quarter-wave DBR, an $Al_{0.22}Ga_{0.78}As$-GaAs-$In_{0.2}Ga_{0.8}As$ resonant λ-cavity, p-doped contact layers, and a 22-pair undoped AlAs/GaAs quarter-wave DBR. The p-doped contact layers are formed from a 0.25 λ AlAs current constriction layer and a 0.75 λ GaAs intracavity contact layer. This structure is good for studying the reflectivity-dependence of laser characteristics by directly changing the pair numbers of the top DBR to vary mirror loss, because the top DBR is composed of binary materials with abrupt interfaces and can be selectively removed one pair at a time. There is also no change in

the current-voltage characteristics caused by reducing the number of top pairs owing to the use of intracavity p-contact.

AlAs native-oxide apertured VCSEL's have been fabricated with various aperture sizes. The aperture size dependence of threshold currents and top emission efficiencies are plotted in Fig.1. Threshold current reduces with decrease of current aperture size from 10x10 μm^2 to 3x3 μm^2, where I_{th} reaches its minimum value of 100 μA. With further decrease of aperture size, threshold current goes up. Particularly, from 2x2 μm^2 to 1x1 μm^2, I_{th} increases significantly from 150 μA up to 940 μA. It is also seen that the external quantum efficiency of top emission decreases with the reduction of aperture size, particularly, a dramatic change in the range of small aperture sizes. The change of external quantum efficiency with aperture size indicates that when aperture gets smaller, internal quantum efficiency decreases, and round trip loss increases. The pictures of laser beam spot in Fig.1 are the far-field patterns for devices with various aperture sizes, showing dependence of lateral confinement for optical mode on aperture size.

For in-plane edge-emitting lasers, the internal quantum efficiency (η_i) and the internal loss (α) can be estimated by fitting the reciprocal external quantum efficiency (η_d^{-1}) vs the cavity length (L), using

$$\frac{1}{\eta_d} = \frac{1}{\eta_i} + \frac{\alpha}{\eta_i \ln(1/R)} \cdot L \qquad (1)$$

Similarly, using L-I data of VCSEL's with different reflectivity, we can evaluate important parameters associated with VCSEL's. Instead of fitting $(1/\eta_d)$~L as in edge-emitter case, the data of $(1/\eta_d)$~1/ln(1/R) are used because the cavity length for a VCSEL is fixed. The corresponding equation for VCSEL's is

$$\frac{1}{\eta_d} = \frac{1}{\eta_i} + \frac{A}{\eta_i} \cdot \left(\frac{1}{\ln(1/R)} \right) \qquad (2)$$

where A is the round-trip loss in a VCSEL, R is the total power reflectivity. The term 1/ln(1/R) is so sensitive to the value of R, especially, when R is in the range of 0.9990-0.9999, 1/ln(1/R) changes with R dramatically. Therefore, such fitting to obtain values of η_i and A for VCSEL's is much more difficult than that for edge-emitting lasers.

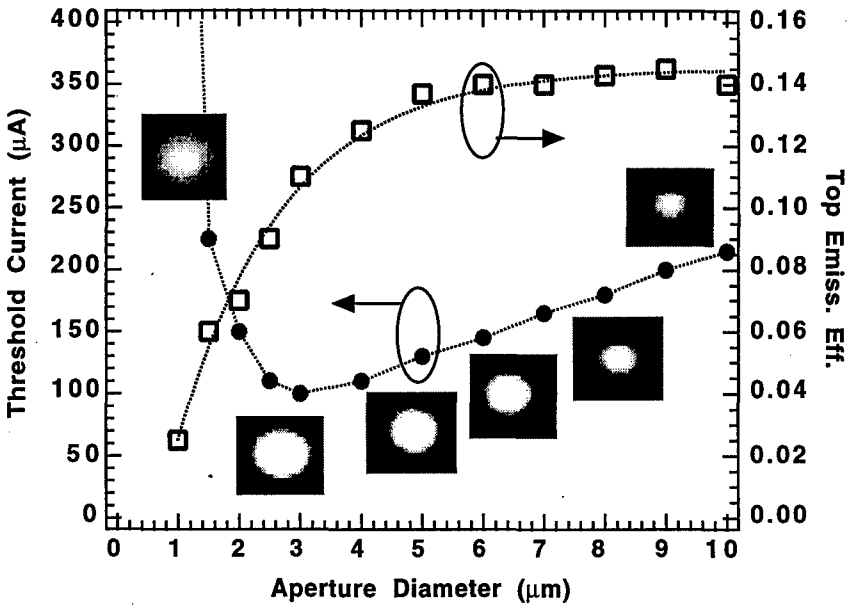

Figure 1 - The aperture size dependence of threshold currents and top emission efficiencies. The pictures of laser beam spot are the far-field patterns for devices with various aperture sizes. showing dependence of lateral confinement for optical mode on aperture size.

Prior to removing layers on top mirror, the devices are patterned so that only the top mirror and part of the contact pad are exposed for etching and probing, respectively, as schematically shown in Fig. 2. The VCSEL's devices were finished with top mirrors of 25x25 μm^2 sizes. An 15x15 μm^2 opening window is applied on the top mirror. To protect device structure from wet etching, a thick layer of photoresist AZ4620 (~6 μm) is used.

Etching starts with buffered-oxide-etchant (BOE) to remove possible oxide layer on the mirror top. Then, a solution of $NH_4OH:H_2O_2$/1:4 is used to selectively remove GaAs over AlAs, and BOE to selectively etch AlAs over GaAs. Each step has to be carefully controlled by monitoring mirror surface and L-I measurement. Reliable data should be acquired when mirror surface looks very clean and L-I curve remains unchanged for further same etching. This is very crucial to the experiment. It is also important to have all the L-I measurement taken at same conditions for accurate comparison.

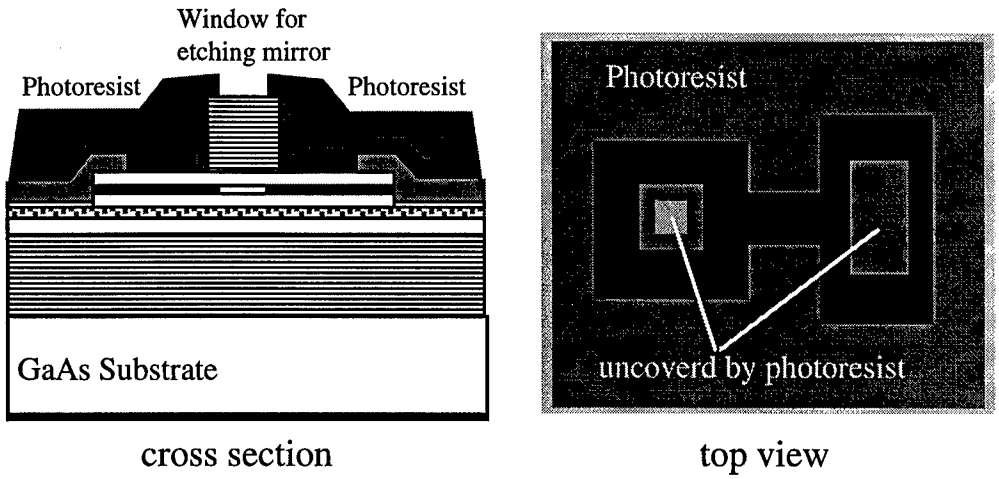

Figure 2 - Schematic of VCSEL's device covered with photoresist mask for removing top DBR by pairs to vary reflectivity of top mirror.

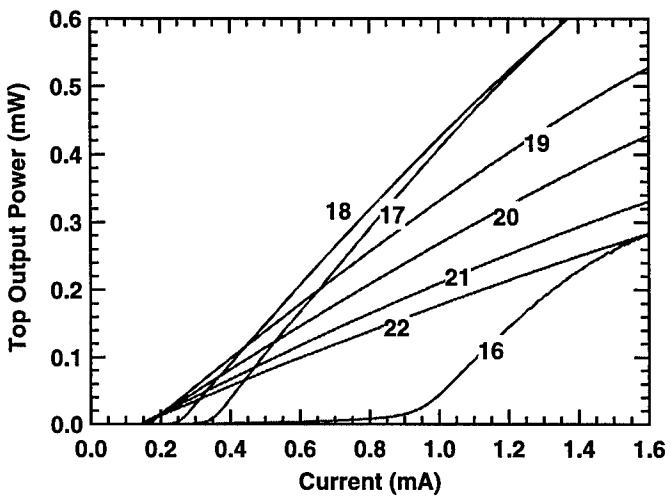

Figure 3 - A typical result of L-I curves for a VCSEL with various number of DBR pairs as top mirror.

An etching experiment to remove layers of the top DBRs on the VCSEL's devices with various current aperture sizes on same wafer has been carefully carried out. A typical result of L-I curves for a VCSEL with various number of DBR pairs as top mirror is shown in Fig.3. The numbers shown on thecurves indicate the pairs of the top mirror at which the L-I curves were taken. With decrease of reflectivity by removing layers in top mirror, both threshold current and external quantum efficiency increase resulting from increases of mirror loss. This is similar to that reported earlier by G.M. Yang *et al* . [7]

To fit $(1/\eta_d)$~1/ln(1/R), reflectivity $R = \sqrt{R_t \cdot R_b}$ has to be determined first, where R_t, R_b are reflectivities of top and bottom mirrors viewed from inside cavity. Experimentally, it is impossible to measure those values for the devices. In our experiment, we assume reflectivities are reasonably same for all size devices, and it applies to each step of uniform etching. Using L-I data of one device, assuming certain numbers for its internal quantum efficiency (η_i) and round trip loss (A), to calculate values of ln(1/R), we then fit data of other size devices with those R values to obtain data of η_i and A. Normalized ratios of η_i and A for those devices can illustrate the aperture size effect on internal quantum efficiency and round trip loss.

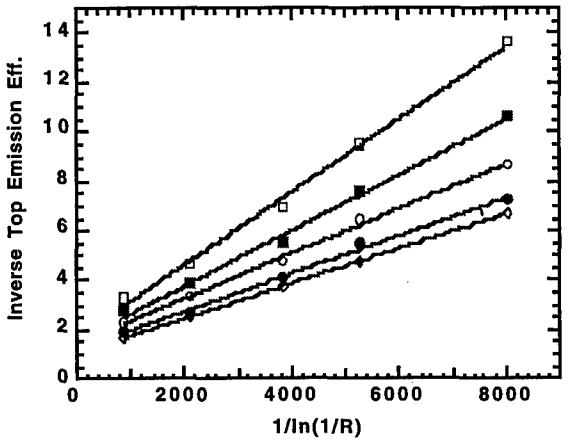

Figure 4 - The data fitting of inverse external quantum efficiency of top emission to 1/ln(1/R) for devices with various aperture sizes.

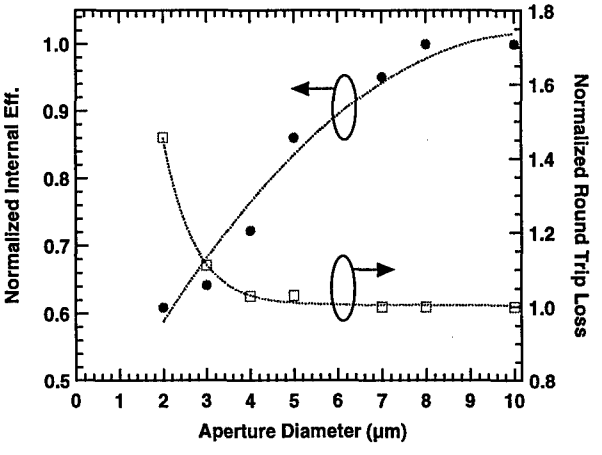

Figure 5 - The dependence of normalized ratios of internal quantum efficiency and round trip loss on current aperture size.

Fig.4 shows the data fitting of inverse external quantum efficiency of top emission to 1/ln(1/R) for devices with various aperture sizes, assuming η_i = 95% and A = 0.0007 for 10 x10 μm^2-size device as reference. Those five points on each device correspond to top mirrors with 22, 21, 20, 19 and 18 pairs of GaAs/AlAs DBR's.

In Fig.5, dependence of normalized ratios of internal quantum efficiency and round trip loss on current aperture size is shown. With reduction of aperture size, internal quantum efficiency decreases and round trip loss increases, in other words, both carrier loss and optical loss increase. It is noted that with change of aperture size from 10 x 10 μm^2 to < 2 x 2 μm^2, the internal quantum efficiency begins to drop at < 7 x 7 μm^2, and down by 50% at < 2 x 2 μm^2; while round trip loss begins to increase when aperture size is less than 3 x 3 μm^2, and up by 40% at <2 x 2 μm^2.

Our experiment has demonstrated that with reduction of current aperture size of AlAs native-oxide confined VCSEL's, the internal quantum efficiency decreases and the round trip loss increases. Generally, a reduction of internal quantum efficiency results from currents which continue to increase above threshold. In our VCSEL's structure, carrier loss may occur through several ways such as spreading current in cladding layers, carrier out-diffusion in the quantum well layer, carrier trapping by interface states between oxidized and non-oxidized materials, etc. Such effect of carrier loss is should be expected more significant for smaller aperture size. Optically, round-trip loss increases with reduction of aperture size is due to excess diffraction and scattering loss.

The fitting technique itself, as shown in Eq. (2), is limited for accurately achieving absolute values of internal quantum efficiency and round trip loss by the sensitivity of the term 1/ln(1/R) to the value of R in the range of 0.9990-0.9999 [9]. Since it is impossible to experimentally measure reflectivities of top and bottom mirrors viewed from inside cavity, using theoretically calculated values of $R=\sqrt{R_t \cdot R_b}$ for fitting can result in errors unless both grown layers of DBR's are exactly quarter-wavelength thicknesses and the data of refractive index in the library for calculation are very accurate. To avoid such difficulty, instead of determining absolute values of internal quantum efficiency and round trip loss, we chose to study the relative comparison of those values for devices with various aperture size, in our experiment, to emphasize the aperture size effect on lateral confinement for carriers and optical mode. One possible error may be introduced in Fig.4 is that total emission efficiency should have been used for the fitting rather than top emission efficiency. To do so, determination of R_t, R_b has to be involved. However, we think such correction can not be so strong to alter the dependence of internal quantum efficiency and round trip loss on current aperture size.

In conclusion, we present here an experimental characterization of current aperture size effect on internal quantum efficiency and round trip loss of AlAs native-oxide confined VCSEL's. It has been demonstrated that with reduction of aperture size to less than 5 x 5 μm^2, the internal quantum efficiency decreases owing to carrier losses resulting from current spreading and carrier out-diffusion, the round-trip loss increases due to excess diffraction and scattering losses. In addition to excess optical losses [5,8], we believe and demonstrate in this paper that the effect of carrier loss in native-oxide apertured VCSEL's is also significant and limits the scaling down of device performance with aperture size for most reported VCSEL's confined by native-oxide so far, which have no intentional lateral confinement for carriers in the layers below current aperture.

References:

[1] Y. Hayashi, T. Mukaihara, N. Hatori, N. Ohnoki, A. Matsutani, F. Koyama, and K. Iga, "Record low-threshold index-guided InGaAs/GaAlAs vertical-cavity surface-emitting laser with a native oxide confinement structure", *Electron. Lett.* , 30(7), pp560-561 (1995).
[2] K.L. Lear, K.D. Choquette, R.P. Schneider, Jr., S.P. Kilcoyne, and K.M. Geib, "Selectively oxidised vertical cavity surface emitting lasers with 50% power conversion efficiency", *Electron. Lett.* , 31(3), pp208-209 (1995).
[3] G.M. Yang, M.H. MacDougal, and P.D. Dapkus, "Ultralow threshold current vertical-cavity surface-emitting lasers obtained with selective oxidation", *Electron. Lett.*, 31(11), pp886-888 (1995). [4] D.L. Huffaker, L.A. Graham, H. Deng, and D.G. Deppe, "Sub-40μA continuous-wave lasing in an oxidized vertical-cavity surface-emitting laser with dielectric mirrors", *IEEE Photon. Technol. Lett.* , 8, pp974-976 (1996).
[5] E.R. Hegblom, D.I. Babic, B.J. Thibeault, and L.A. Coldren, "Estimation of scattering losses in dielectrically apertured vertical cavity lasers", *Appl. Phys. Lett.* 68(13), pp.1757-1759, (1996).
[6] Yong Cheng, and P.D. Dapkus, "Confinement Effects of AlAs Native-Oxide Apertures Buried in Edge-Emitting Lasers and Vertical-Cavity Surface-Emitting Lasers", submitted to *EEE Photon. Technol. Lett.* .
[7] G.M. Yang, M.H. MacDougal, V. Pudikov, and P.D. Dapkus, "Influence of mirror reflectivity on laser performance of very-low-threshold vertical-cavity surface-emitting lasers", *IEEE Photon. Technol. Lett.* , 7(11), pp1228-1230 (1995).
[8] T.-H. Oh, D.L. Huffaker, and D.G. Deppe, "Size effects in small oxide confined vertical-cavity surface-emitting lasers", *Appl. Phys. Lett.* 69(21), pp.3152-3154, (1996).
[9] Yong Cheng, "Design, fabrication and characterization of high-performance Native-Oxide Confined InGaAs/GaAs Quantum-Well Edge-Emitting and Surface-Emitting Lasers", Ph.D Dissertation, University of Southern California, 1997.

III. Effect of Scaling Microlasers on Modal Noise:

Microlasers will find use in future waveguide-based communication systems. Such systems will use multimode optical waveguide media and as such will be subject to performance limitations imposed by modal noise. Modal noise is unwanted random variation in received light intensity stemming from interference effects in multimode waveguide. It was first described by R. Epworth in 1978 [1] and later Kanada [2], Dandliker et al. [3], and Bates et al. [4] studied modal noise in systems which made use of conventional laser diode sources. Hahn et al. [5] recognized modal noise from coherent microlaser emission could be reduced using large area multi-transverse mode Vertical Cavity Surface Emitting Lasers (VCSELs). Despite recent interest in the subject, the behavior of modal noise in scaled lasers and microlasers has not been systematically evaluated

We have investigated the effects of scaling microlasers on modal noise for a 1 Gb/s optical communication system using multimode waveguides. The length of multimode optical waveguide considered varies from 10 cm to 1 km and the waveguide itself has a 1 GHz.km modal bandwidth. We numerically solve the multimode laser diode rate equations and obtained the spectra of the laser for different electrical modulation conditions, laser diode cavity size, and spontaneous emission factor. To simulate the performance of Gb/s optoelectronic interconnects, we model a detector with 1 GHz -3 dB high-frequency roll-off as a weighted time average of the received light intensity. We use speckle visibility at the end of a length L of multimode waveguide as our measure of modal noise.

Decreasing the laser cavity length, L_C, causes the spectrum to be increasingly single mode, thereby increasing coherence, visibility, and modal noise. This initial consideration indicates that micro-lasers have a higher susceptibility to modal noise and may not be suitable for high-speed optoelectronic communication systems. However, we also found that the visibility due to a digitally modulated single-mode microlaser can be reduced because the time averaged optical spectra exhibits two spectral peaks which has the effect of reducing optical coherence. This decrease in coherence of microlaser optical emission reduces modal noise. We have found that by optimizing the operating conditions of the microlaser, it is possible to reduce modal noise to levels comparable to those found in conventional laser diodes. Further, in stark contrast to conventional lasers, micro-lasers with large spontaneous emission factors, show lack of carrier pinning and have lower visibility values when the steady-state bias current is increased for a given depth of modulation current.

From results of our work shown in Fig.1, one may see that for a given bias current and depth of modulation, conventional lasers with cavity length $L_C > 50$ μm are suitable for multimode waveguide communication over lengths less than 1 m. However, low threshold current, low-power microlasers with optimized design and operating conditions perform as well as conventional high threshold current, large, incoherent multimode devices

Modal noise and speckle visibility in Gb/s multimode waveguide interconnect systems depends on a complex interplay of carrier dynamics, spontaneous emission factor, gain compression, and device dimensions. These competing factors allow scaled low-power microlasers with optimized design and operating conditions to exhibit modal noise comparable to large incoherent multimode devices.

Part of this work is described in a paper "The effect of scaling microlasers on modal noise" by S. M. K. Thiyagarajan and A. F. J. Levi, which has been published in Appl. Phys. Lett. **69**, 3459-3461 (1996).

References:

[1] R. E. Epworth, in Proceedings of the Fourth European Conference on Optical Communication (Istituto internazionale delle communicazioni, Genova, Italy, 1978), pp. 492-501.
[2] T. Kanada, J. Lightwave Tech. **2**, 11 (1984).
[3] R. Dandliker, A. Bertholds and F. Maystre, IEEE J. Lightwave Tech. **3**, 7 (1985).
[4] R. J. S. Bates, D. M. Kuchta and K. P. Jackson, Optical and Quantum Electron. **27**, 203 (1995).
[5] K. H. Hahn, M. R. Tan, Y. M. Houng and S. Y. Wang, Electron. Lett. **29**, 1482 (1993).

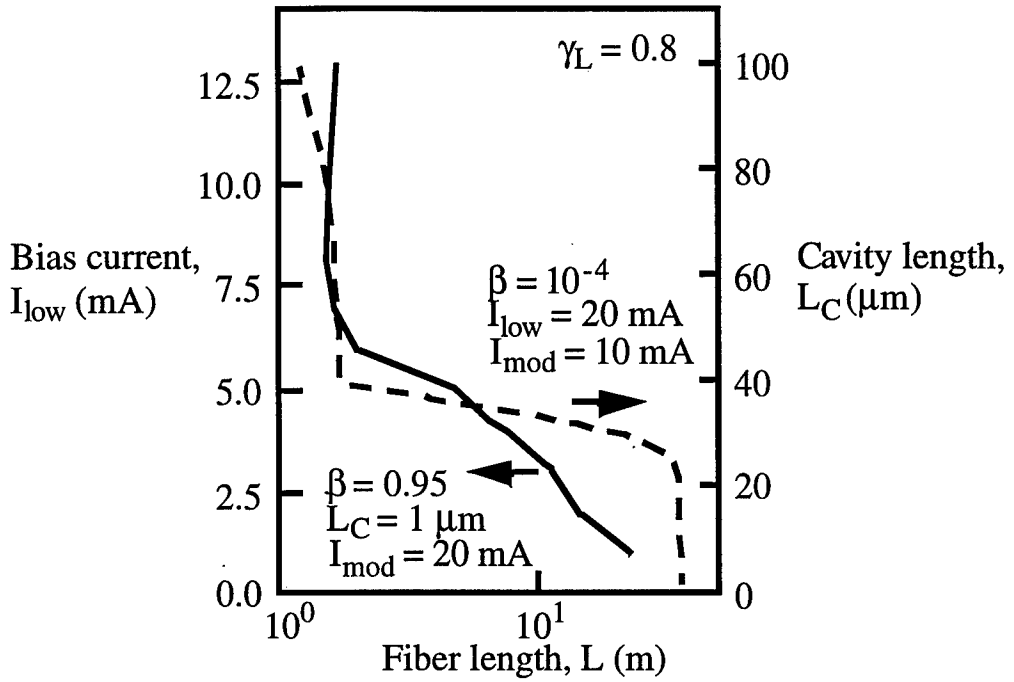

Figure 1 - Dependence of the multimode waveguide length, L at which visibility $\gamma_L = 0.8$. The figure shows the dependence on the steady-state bias current, I_{low}, of a microlaser with spontaneous emission factor $\beta = 0.95$ (solid line) and the dependence on laser diode cavity length, L_C, for a device with $\beta = 10^{-4}$ (dashed line).

IV. Series resistance of microlasers:

The experimental portion of this program involves fabrication of VCSELs with active areas less than 1 μm x 1μm. We have derived analytical expressions for the extrinsic series resistance in intracavity-contacted VCSELs that illustrate the contributions to series resistance of various portions of the device. To test the validity of these expressions low resistance, low threshold-current, intracavity-contacted VCSELs have been fabricated with increased doping in the contact layer of the p- region to examine the tradeoffs that arise if we depart from our previous designs with low loss and low threshold. Resistances ranging from 355 Ω for 4 μm square apertures to 80 Ω for 12 μm square apertures and threshold voltages as low as 1.35 V have been obtained. The threshold currents range from 270 μA for 4 x 4 μm apertures to 850 μA for 12 x 12 μm. The measured data agrees well with the analytical, demonstrating the validity of this derivation.

Figure 1 depicts a typical structure that employs intracavity contacts for current injection into the active region. The structure shown has oxide DBRs [4,6,9] for reflectors, but the analysis here could as well apply to intracavity contacted structures with all-semiconductor DBRs [1,5,10] or deposited thin-film DBRs [2,3,7].

The region between the mirrors consists of an active region bounded by the p-type and n-type contact layers. The active region consists of 2 $In_{0.2}Ga_{0.8}As$ quantum wells with GaAs barriers bounded by $Al_{0.25}Ga_{0.75}As$ to form a single wavelength cavity. The p-contact layer is a single Bragg pair made up of a graded interface GaAs/AlAs pair. The GaAs is divided into a highly doped and a low doped region to promote current spreading across the aperture [11]. The n-contact layer is similar except that a current spreading layers is not needed since electrons have a much higher mobility. Layer thicknesses and dopings are listed in Table I.

To analyze the resistance, the contact layer is split into 3 regions as shown in Fig. 2. Region A represents the resistance of injecting carriers from the metal into the semiconductor. Region B represents the resistance of carriers moving from the metal to the aperture edge. Region C represents the resistance of carriers moving through the current spreading region and the aperture.

Expressions for resistance have been derived for the p-contact layer since it dominates the resistance of the device, but they may be similarly applied to the n-contact layer using the n-AlAs layer as the current spreading layer. Although we assume a cylindrical geometry, our standard mask set is based on square geometries. Thus, there will be some error when comparing experimentally measured data and calculated data. To reduce the error and closely approximate square geometries, the ratio between the perimeter(circumference) and width (diameter) is changed from π to 4.

Devices with the specifications enumerated in Table I have been grown and fabricated. The growth and fabrication of this device is similar to previous devices [6] except that the doping of the p-contact layer has been increased and an alloyed Ag/Zn/Ag contact has been used to form an ohmic contact. With these changes, we have obtained voltages as low as 1.35 V and resistances as low as 80 Ω. Elimination of resistance at the heterojunctions by composition grading is indicated by the low threshold voltage which is only 100 mV greater than the photon energy (λ = 991 nm) and very close to the record for 980 nm VCSELs [12]. Fig. 3 shows the L-I-V curves for several different sizes of representative devices taken at room temperature under cw excitation. The differential series resistance at $I > 10^*I_{th}$ are 355 Ω, 200 Ω, 140 Ω, and 80 Ω, which correspond to threshold currents of 270 μA, 300 μA, 500 μA, and 850 μA, respectively. The high bias ensures that the diode is fully turned on and,thus, adds little differential resistance to the total. The total resistance for the same device is calculated taking into account both the p-type contact layer and the n-type contact layer, and it is plotted against the measured data in Fig. 4. The calculated data predicts the experimental data quite closely. This validates the analytic model and enables us to predict structures with different layer thicknesses and dopings.

The calculated resistances from the different regions are presented in Fig. 5 as a function of oxide aperture width. The resistance in region A (contact resistance) is

6.9 Ω. At moderate aperture widths from 16 μm to 5 μm, the resistances from regions B and C are approximately the same, increasing as the aperture width decreases. At 5 μm, R_C begins to rise dramatically and at 2 μm the resistance is almost 1000 Ω. The origin of this is the small area of the current constriction in combination with the low doped current spreading layer. It may be possible to remove the spreading layer without suffering adverse effects at small aperture sizes since current spreading becomes less of an issue. Nonetheless, the resistance will still rise as dimensions decrease. In any case, the increased resistance for small apertures must be reduced in order that the ultralow threshold currents obtained may be used for high speed applications.

In summary, we have derived expressions for the resistance in intracavity contacted VCSELs. We have demonstrated the validity of these expressions by fabricating low resistance, low threshold-current, intracavity-contacted VCSELs. Using these equations, it is possible to quickly calculate the extrinsic series resistance and determine its origin during the design process, rather than waiting to measure it in the more expensive and time-consuming fabrication process.

References:

[1] J. W. Scott, B. J. Thibeault, D. B. Young, L. A. Coldren, and F. H. Peters, "High efficiency submilliamp vertical cavity lasers with intracavity contacts", *IEEE Photonics Technology Letters*, **6**, 678 (1994).

[2] D. L. Huffaker, D. G. Deppe, K. Kumar, and T. J. Rogers, "Native-oxide defined ring contact for low threshold vertical-cavity lasers", *Applied Physics Letters*, **65**, 97 (1994).

[3] D. L. Huffaker, J. Shin, and D. G. Deppe, "Low threshold half-wave vertical-cavity lasers", *Electronics Letters*, **30**, 1946 (1994).

[4] M. H. MacDougal, P. D. Dapkus, V. Pudikov, H. Zhao, and G. M. Yang, "Ultralow threshold current vertical-cavity surface-emitting lasers with AlAs oxide/GaAs distributed Bragg reflectors", *IEEE Photonics Technology Letters*, **7**, 229 (1995).

[5] G. M. Yang, M. H. MacDougal, and P. D. Dapkus, "Ultralow threshold current vertical-cavity surface-emitting lasers obtained with selective oxidation", *Electronics Letters*, **31**, 886 (1995).

[6] M. H. MacDougal, G. M. Yang, A. E. Bond, C. K. Lin, D. Tishinin, and P. D. Dapkus, "Electrically-pumped vertical-cavity lasers with Al_xO_y-GaAs reflectors", *IEEE Photonics Technology Letters*, **8**, 310 (1996).

[7] D. L. Huffaker, L. A. Graham, H. Deng, and D. G. Deppe, "Sub-40μA continuous-wave lasing in an oxidized vertical-cavity surface-emitting laser with dielectric mirrors", *IEEE Photonics Technology Letters*, 8, 974 (1996).

[8] J. W. Scott, "Design, fabrication and characterization of high-speed intra-cavity contacted vertical-cavity lasers", Ph. D. dissertation, University of California at Santa Barbara (1995).

[9] M. H. MacDougal, H. Zhao, P. D. Dapkus, M. Ziari, and W. H. Steier, "Wide-bandwidth distributed Bragg reflectors using oxide/GaAs multilayers", *Electronics Letters*, **30**, 1147 (1994).

[10] G. M. Yang, M. H. MacDougal, V. Pudikov, and P. D. Dapkus, "Influence of mirror reflectivity on laser performance of very low threshold vertical-cavity surface-emitting lasers", *IEEE Photonics Technology Letters*, **7**, 1228 (1995).

[11] J. W. Scott, R. S. Geels, S. W. Corzine, and L. A. Coldren, "Modeling temperature effects and spatial hole burning to optimize vertical-cavity surface-emitting laser performance", *IEEE Journal of Quantum Electronics*, **29**, 1295 (1993).

[12] K. D. Choquette, R. P. Schneider Jr., K. L. Lear, and K. M. Geib, "Low threshold voltage vertical-cavity lasers fabricated by selective oxidation", *Electronics Letters*, **30**, 2043 (1994).

Table I - Constants and variables used for calculations.

Variable	symbol	value used
highly doped p-GaAs thickness	t_h	0.36 μm
highly doped p-GaAs doping		2×10^{18} cm^{-3}
highly doped p-GaAs resistivity	ρ_h	2×10^{-2} Ω-cm
low doped p-GaAs thickness	t_l	0.12 μm
low doped p-GaAs doping		1×10^{16} cm^{-3}
low doped p-GaAs resistivity	ρ_l	2 Ω-cm
metal contact resistance	ρ_c	2×10^{-6} Ω-cm^2
outer p-metal radius	r_1	20 μm
inner p-metal radius	r_2	10 μm
p-oxide aperture radius	r_3	variable
n-GaAs thickness	t_h	0.335 μm
n-GaAs doping		1×10^{18} cm^{-3}
n-GaAs resistivity	ρ_h	2×10^{-3} Ω-cm
n-AlAs thickness	t_l	0.060 μm
n-AlAs doping		1×10^{18} cm^{-3}
n-AlAs resistivity	ρ_l	0.21 Ω-cm
outer metal radius	r_1	50 μm
inner metal radius	r_2	35 μm
oxide aperture radius	r_3	p-oxide radius + 2 μm
characteristic length(A)	δ_A	$\sqrt{\rho_c t_h / \rho_h}$
characteristic length(C)	δ_C	$\sqrt{\rho_l t_l t_h / \rho_h}$

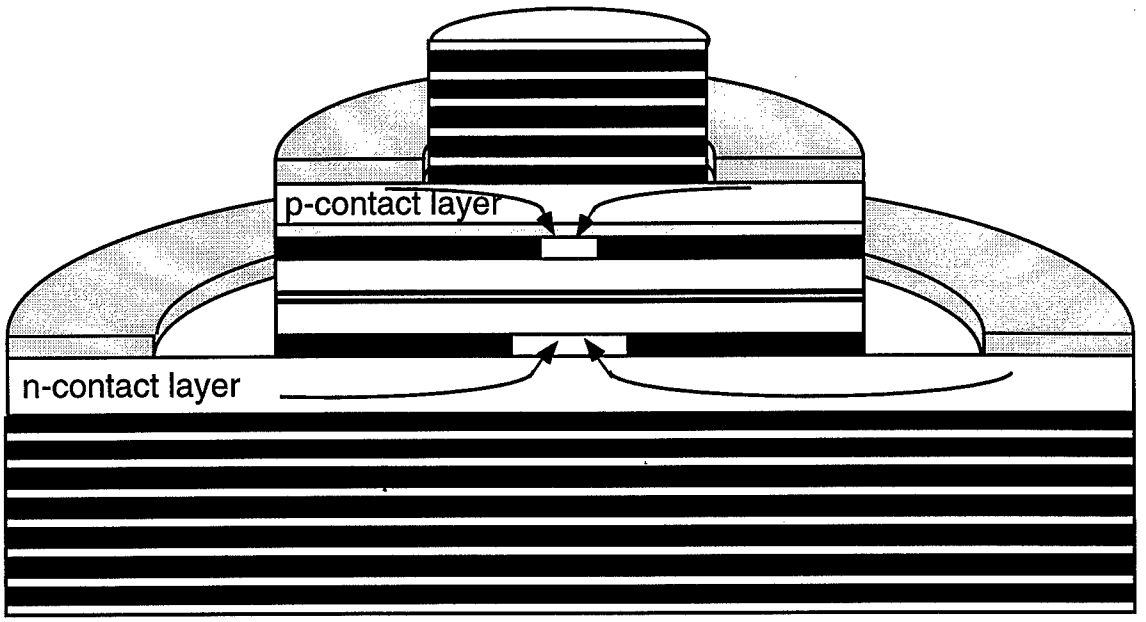

Figure 1 - Schematic of VCSEL used to derive expressions for resistance.

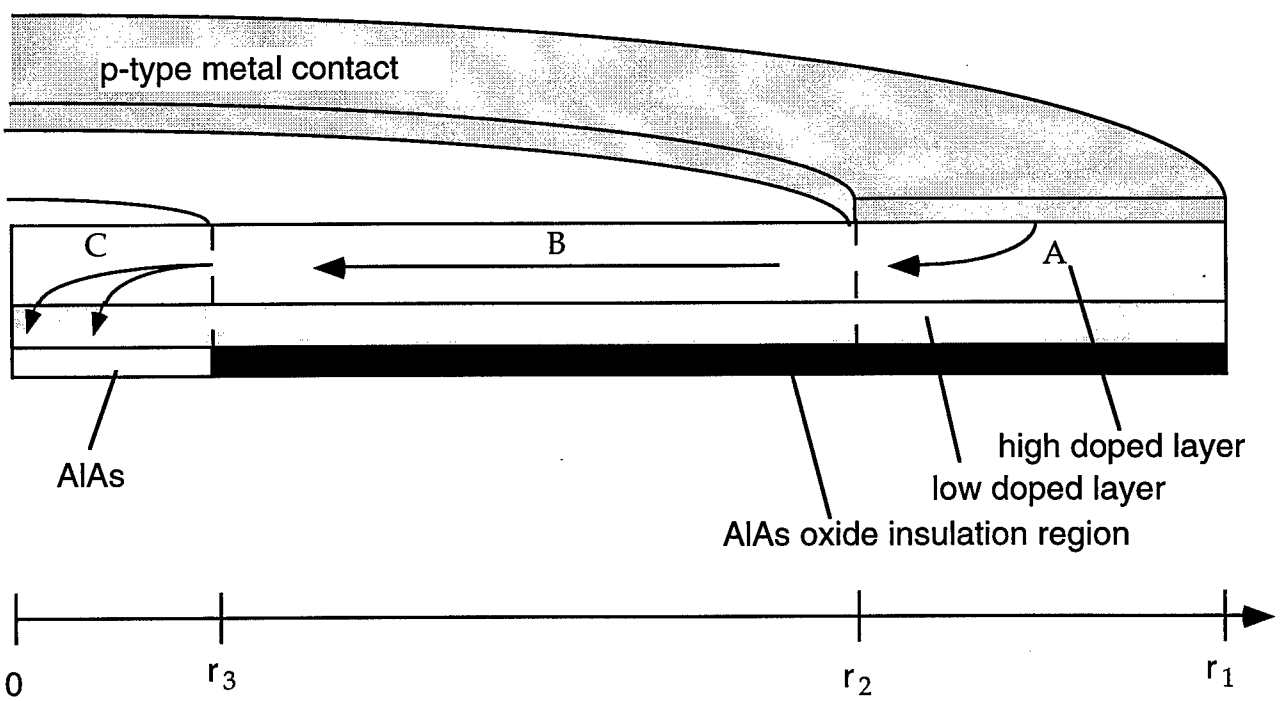

Figure 2 - Schematic of p-doped layer through which current is injected. Different regions represent different modes of current flow. They are defined by different radii, r_1, r_2, and r_3.

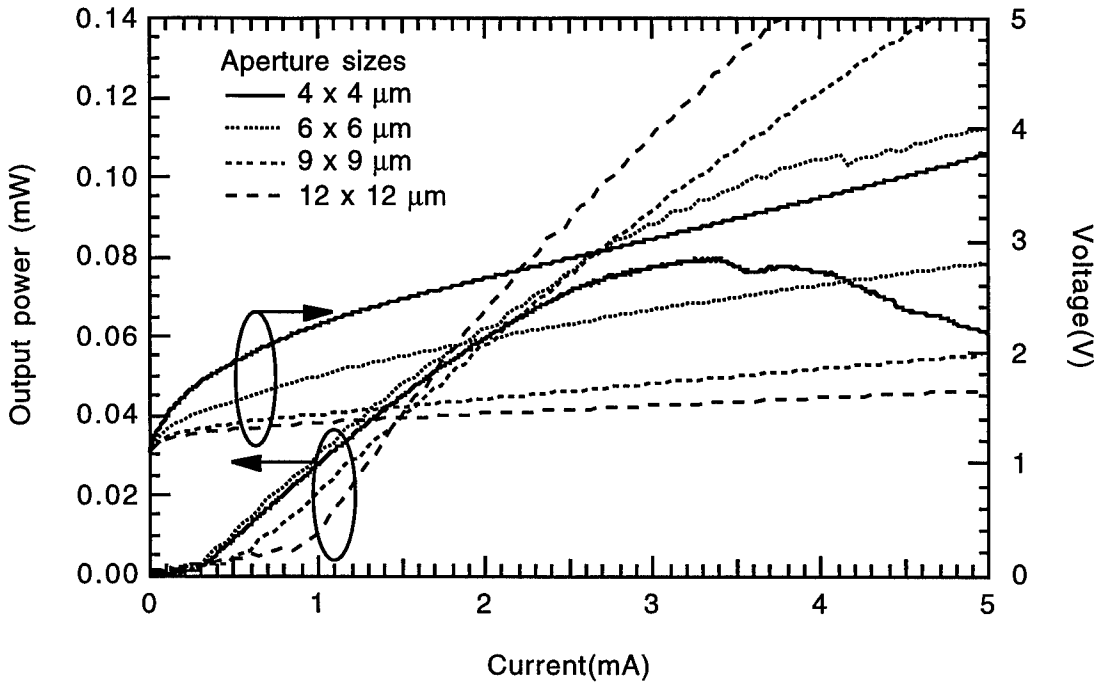

Figure 3 - L-I-V of devices with different oxide aperture sizes. The differential resistance is found by taking the derivative of the I-V curve.

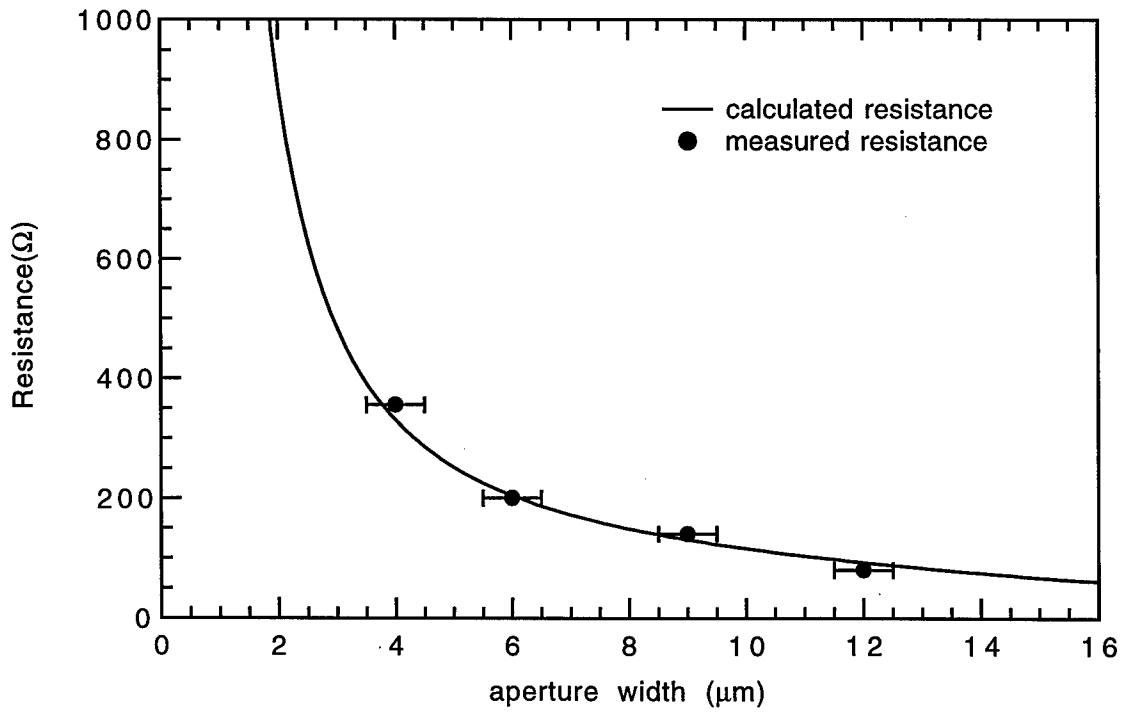

Figure 4 - Comparison of calculated resistance with measured differential series resistance values for different aperture sizes.

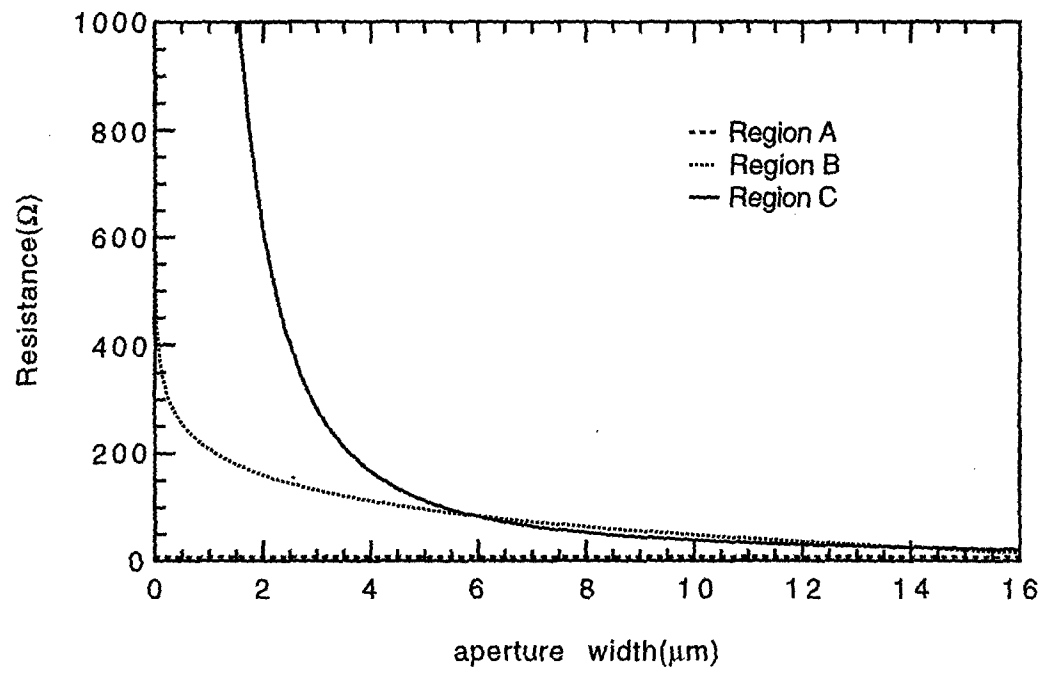

Figure 5 - Calculated resistance contribution of different parts of contact layer as a function of aperture radius for a circular geometry. At the smaller radii, the resistance going through the aperture dramatically increases.